



HAL
open science

Magnetic Resonance Imaging Study of Adipose Tissues in the Head of a Common Dolphin (*Delphinus delphis*): Structure Identification and Influence of a Freezing-Thawing Cycle

Marion Arribart, Julien Ognard, Claude Guintard, Frédéric Domergue, Sami Hassani, Douraied Ben Salem, Jean-Luc Jung

► To cite this version:

Marion Arribart, Julien Ognard, Claude Guintard, Frédéric Domergue, Sami Hassani, et al.. Magnetic Resonance Imaging Study of Adipose Tissues in the Head of a Common Dolphin (*Delphinus delphis*): Structure Identification and Influence of a Freezing-Thawing Cycle. *Anatomia, Histologia, Embryologia*, 2017, 46 (2), pp.204-212. 10.1111/ahe.12258 . hal-02967835

HAL Id: hal-02967835



<https://hal.science/hal-02967835v1>

Submitted on 10 Dec 2024

HAL is a multi-disciplinary open access archive for the deposit and dissemination of scientific research documents, whether they are published or not. The documents may come from teaching and research institutions in France or abroad, or from public or private research centers.

L'archive ouverte pluridisciplinaire **HAL**, est destinée au dépôt et à la diffusion de documents scientifiques de niveau recherche, publiés ou non, émanant des établissements d'enseignement et de recherche français ou étrangers, des laboratoires publics ou privés.

Magnetic Resonance Imaging Study of Adipose Tissues in the Head of a Common Dolphin (*Delphinus delphis*): Structure Identification and Influence of a Freezing–Thawing Cycle

M. Arribart^{1a}, J. Ognard^{2a}, C. Guintard¹, F. Domergue³, S. Hassani⁴, D. Ben Salem²  and J.-L. Jung^{5*} 

Addresses for authors: ¹ Service d'anatomie comparée, Ecole Nationale Vétérinaire ONIRIS, 102 Route de Gachet, 44300 Nantes, France;

² Service d'Imagerie Forensique, LaTIM - INSERM UMR 1101, Université de Bretagne Occidentale, CHRU Brest, Boulevard Tanguy Prigent, 29609 Brest Cedex, France;

³ Laboratoire de Biogenèse Membranaire, UMR 5200, Université de Bordeaux, 71 Avenue Edouard Bourlaux, 33883 Villenave d'Ornon Cédex, France;

⁴ Laboratoire d'étude des mammifères marins - Océanopolis, Port de Plaisance du Moulin Blanc, 29200 Brest, France;

⁵ Laboratoire BioGeMME, Université de Bretagne Occidentale et Université Bretagne Loire - UFR Sciences et Techniques, 6 ave Le Gorgeu, 29200 Brest, France

Co-first authors.

*Correspondence:

Tel.: +33298016129;

fax: +33298016311;

e-mail: jung@univ-brest.fr

Summary

Magnetic resonance imaging (MRI) was used to scan the head of a common dolphin (*Delphinus delphis*) in order to visualize the different adipose tissues involved in echolocation functioning and to precisely delineate their anatomical topology. MRI scans were performed on the head taken from a freshly stranded carcass and repeated after a 2-week freezing time followed by thawing. The main fatty organs of the head, that is the melon, the *mandibula bulba*, the *bursae cantantes*, and their different connections with surrounding tissues were identified and labelled. The nasal sacs, other organs of echolocation, were also identified and labelled thanks to different MRI acquisitions. The shape, the location, the type of MRI signal of each organ and of their different connections were successfully analysed on all images, and then, the images of the head fresh or after thawing were compared. No impacts of the freezing/thawing cycle on the fatty tissues of the head were identified. Different parts were distinguished in the melon on the basis of the MRI signal emitted, corresponding most likely to the internal and external melon already identified by other analytical approaches, and linked to differences in lipid composition. MRI is shown here to be a useful tool to study the functional anatomy of the organs responsible for echolocation in odontocetes, with a particularly high level of precision.

Introduction

Among mammals, cetaceans have a highly specific lipid metabolism. Two types of specialized and organized adipose tissues allow them to achieve biological and physiological functions of major importance for their adaptation to the marine environment. First, a layer of subcutaneous adipose tissue (called 'blubber', found in all cetaceans) provides insulation and buoyancy (Koopman et al., 2002; Bagge et al., 2012). The second type of highly

specialized adipose tissue, the melon, is only present in odontocetes, whose hunting techniques are more focused due to echolocation, a sense that is almost specific to them (Klopper et al., 2012). This sense is based on the emission through the melon of clicks generated by the MLDB (monkey lips–dorsal bursae) complex (Cranford et al., 2011). The echoes from these sounds, picked up by an internal fat deposit of the mandible, allow odontocetes to analyse the environment and follow their prey. Both adipose tissues are characterized by specific biochemical

topologies and lipid compositions, clearly related to their functions (Koopman, 2007; Koopman and Zahorodny, 2008). In particular, they contain large amounts of branched short-chain fatty acids (FA) such as isovaleric acid (IVA, five carbon atoms) or longer chain FA such as isopalmitic acid (16 carbon atoms). Some odontocetes are also capable of producing wax esters (WE), that is alcohol and FA esters (Litchfield et al., 1975; Koopman, 2007).

In the melon, acoustic fats, that is containing mainly short and branched FA (*i*-FA), are concentrated on an area, the 'central' melon (Litchfield et al., 1973) whose function is to conduct and focus sounds from the MLBD complex to the external environment (Gardner and Varanasi, 2003; Koopman and Zahorodny, 2008; McKenna et al., 2012). Acoustic fats are thought to lower the velocity of sounds (Blomberg, 1978). Their location in the internal part of the melon could therefore explain how the organ serves as a positive acoustic lens (tissues with a low sound velocity being surrounded by higher sound velocity tissues, with longer and less branched FA).

Therefore, delineating the precise anatomical topology of the adipose tissues in odontocetes, taking into account the functionality of the organs, requires to distinguish between soft tissues differing mainly by their lipid composition, and to be able to identify precisely their connection with other tissues (other soft tissues, skeleton, auditory complex, etc.). Medical imaging techniques, in particular magnetic resonance imaging (MRI), are particularly relevant to study soft tissue anatomy. As non-invasive techniques, they allow to observe internal anatomical structures without spatial distortion and/or loss of resolution that can be associated with dissection or sectioning. Because MRI is dependent on tissue biochemical composition, it can be optimized to highlight biochemical differences between tissues, even if they are anatomically indistinguishable from each other (Régis-Arnaud et al., 2011; Genu et al., 2014). MRI therefore offers an innovative approach to draw the compositional topography of adipose tissues of odontocetes, with a much higher level of accuracy than previously possible.

The objective of this study was to determine (1) whether MRI could be used to decipher the complex anatomical structure of the melon and jaw acoustic fats of odontocetes, their connections with surrounding tissues, and (2) whether the resolving power of MRI was sufficient to distinguish between adipose tissues according to their lipid composition, on which their function depends. We analysed an adult female common dolphin (*Delphinus delphis*) stranded dead in the north-west of France, whose carcass was found shortly after stranding. To optimize future experiments, particular attention was also given to possible influence of a freezing–thawing cycle of the carcass on the MRI analysis.

Materials and Methods

Studied animals

A common dolphin (*Delphinus delphis*) was found stranded dead on 23 January 2013 by a correspondent of the French stranding network (described in Jung et al., 2009) along the Atlantic coast in the north-west of France (near the city of Le Guilvinec, 47°47'12"N 4°16'55"W). The carcass was fresh and was determined as a female measuring 138 cm long.

The animal was brought into the laboratory and kept at 4°C for 2 days. The whole head was cut from the body and transported to the CHRU of Brest (*Centre Hospitalier Régional et Universitaire*) where it was analysed by MRI. Immediately after analysis, the head was frozen at –20°C for 2 weeks then thawed, brought slowly to room temperature and analysed again using a same protocol.

MRI acquisition and analysis

The study was performed on a 3T MR 60-cm bore scan Achieva dStream (Philips Healthcare, Best, The Netherlands), using a 16-channel torso receiver coil. Images were obtained using the following sequences: isotropic 3D (slice thickness: 1 mm) T1-weighted turbo field echo with sensitivity encoding (TR/TE) (9.4/3.9 ms), isotropic 3D (slice thickness 1.5 mm) T2-weighted turbo spin echo (VISTA) (1118/200 ms), 3D DP VISTA with fat suppression technique using spectral attenuated inversion recovery (SPAIR) (1300/31.7 ms), sagittal T1 IR (6109.7/12 ms, inversion time 400 ms).

Magnetic resonance imaging images were obtained with heads in ventral recumbency.

Magnetic resonance imaging images were visualized and analysed using two DICOM-viewing software (OsiriX imaging software). An MRI interpretation principle (relative signal analysis) was performed. All of the anatomic elements were described in accordance with the official anatomical terminology in the *Nomina Anatomica Veterinaria*.

Evaluation of inter-observer result consistency

To consolidate the comparison of the MRI images (frozen and thawed), three people (MA, JO and Aurore Lambert, a veterinarian member of the BioGeMME Laboratory) analysed independently nine items (Table 1) on MRI images. All images were previously made anonymous by JIJ. The visibility of each item was determined independently by each of the observers.

The concordance between the three observations was measured by a calculation of Cohen's kappa coefficient.

Table 1. Items used for the measurement of inter-observer agreement

Item number	Item description
1	Outer melon
2	Inner melon
3	<i>Mandibula bulba</i>
4	Link between the <i>mandibula bulba</i> and the middle ear
5	<i>Bursae Cantantes</i>
6	Nasofrontal sacs
7	Nasal plugs
8	Vestibular sacs
9	Premaxillar sacs

This coefficient which is measured from 0.6154 to 1 has proven a strong or almost perfect agreement between the three observers (Landis and Gary, 1977).

Results

The fatty tissues (*Textus adiposus*)

Organ identification

In a T1 IR (inversion–recuperation) MRI acquisition, the two main fatty tissues of the head are clearly detected (Fig. 1). The blubber is clearly visible with a common fat signal (from grey to white) and surrounds all of the head's organs except the melon (Fig. 1: 3,4). The melon, located rostrally, lines the forehead. Two distinct parts can be distinguished in the melon. (Fig. 1: 1,2). The rostral part shows a signal of high intensity (intense white), whereas the caudal part shows a lower medium signal (light grey to grey). This last part has a particular dark signal for a fat tissue with these acquisition parameters, certainly reflecting a different tissue composition. The discrimination between these two parts is further emphasized with a DP VISTA acquisition and added colours corresponding to the signal intensity (Fig. 1). These two parts of the melon, rostral and caudal, correspond most likely to, respectively, the outer and inner parts of the melon (Litchfield et al., 1975). The limit between the blubber and the melon is easily distinguished at the level of the upper respiratory system (Fig. 1).

The acoustic path of the reception complex of the sound waves (Ketten, 1992) is medial to mandibles and is lining to the tympanic part of the temporal bone (Fig. 2). This tympanic part of the middle ear (Fig. 2: 3,4,5) is very expanded compared to the tympanic part of the others mammals and is connected to the inner ear (Fig. 2: 6,7,8) (Ognard et al., 2014). The *mandibula bulba* (Read et al., 1997), and its connection with the middle ear, can be clearly depicted on MRI DP/T2 (Fig. 3a) or a

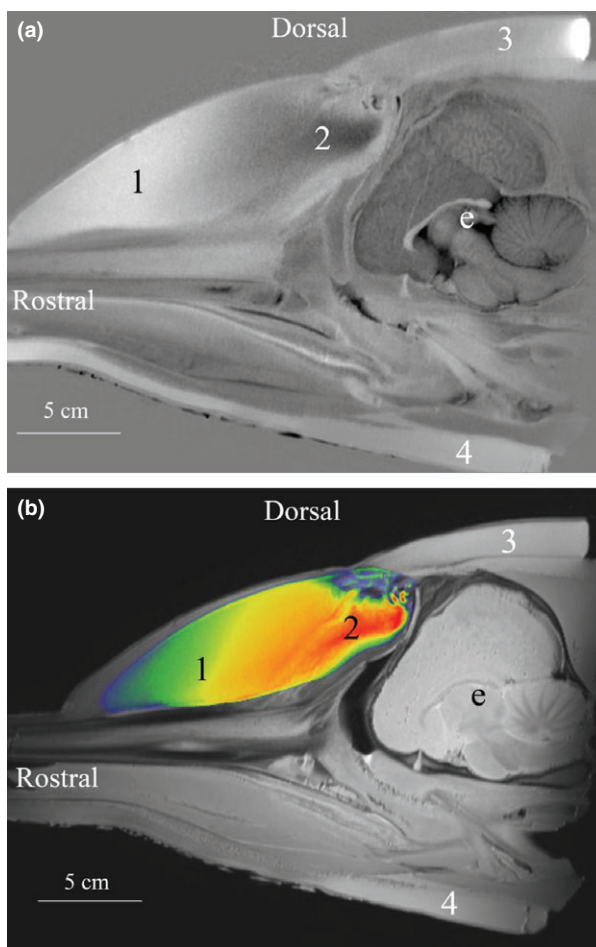


Fig. 1. Two distinct parts of the melon. Parasagittal sections of a fresh common dolphin head (left view). Adipose tissues are highlighted. The compositional heterogeneity of the melon is clearly apparent. (a) T1 IR acquisition. (b) DP VISTA acquisition. Superimposition of colour-coded T1 SE-weighted acquisition of the melon. 1: Outer melon (dorsal part), 2: inner melon (rostral part), 3: dorsal blubber, 4: ventral blubber, e: encephalon. [Colour figure can be viewed at wileyonlinelibrary.com]

T1 SE (Fig. 3b) MRI image where the fatty tissue is appearing with a high-intensity signal (white) and the bones with a very low-intensity signal (black). The connection between the mandibles and the *mandibula bulba* and between the *mandibula bulba* and the tympanic part of the temporal bone is clearly visible on the frontal section, while the covering of the tympanic part of the temporal bone by the *mandibula bulba* is depicted on the sagittal section (Fig. 3).

The *bursae cantantes* (Cranford et al., 2011) are clearly observed with an MPR DP VISTA MRI acquisition (Fig. 4). The frontal section presents the two pairs of horizontal thin organs with a low-intensity signal (quite white). These pairs of fatty tissues are visualized laterally

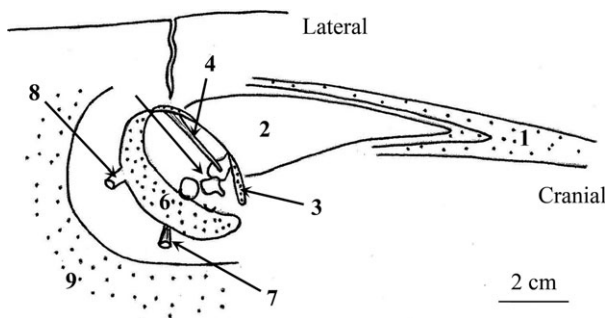


Fig. 2. The odontocete ear. Link between the *mandibula bulba* and the middle ear is highlighted. Synthetic schema. Not real scale. © Marion ARRIBART. 1: Mandibula, 2: *mandibula bulba*, auris media 3: pars tympanica (os temporale), 4; membrana tympani, 5: ossicula auditus (a: malleus, b: incus, b: stapes), auris interna 6: pars petrosal (os temporale) (vestibulum, cochlea), 7: N. vestibulocochlearis, 8: tuba auditiva, 9: os temporale.

to the spiracular cavities (right and left) at the level of the opening of the nasofrontal sac (posterior part).

Lack of influence of a freezing–thawing cycle on the organ shape and MRI signal

The influence of a freezing–thawing cycle was tested by comparing similar MRI acquisitions made before and after freezing of the same common dolphin head. Figure 5 shows the same images as Figs 1, 3 and 4, but acquired after freezing and subsequent thawing of the

whole head. The two parts of the melon are similarly visualized by two different signals in Figs 1 and 5a on the T1 IR acquisition (a stronger white signal for the outer melon and the blubber, a darker signal for the inner melon). The freezing–thawing cycle has also no visible impact on the visualization of the covering of the tympanic part of the temporal bones by the *mandibula bulba* as can be noted by comparing the Figs 3b and 5b. The low-intensity signal of this fatty tissue, as well as the anatomical shape of the organ, is the same before and after freezing. Similarly, the observation of the *bursae cantantes* does not vary before and after freezing, in terms of shape, signal and location (Figs 4b and 5c).

The nasal respiratory system (*Apparatus respiratorius*) and the other main head tissues

The nasal sacs, although difficult to emphasize, are visualized on several different MRI acquisitions. They are filled with air and therefore appear on MRI images with a very low-intensity signal (dark). Nasal diverticula, which are empty, are collapsed, making their visualization difficult. The vestibular sacs are clearly distinguished on a T1 IR image (Fig. 6), while premaxillar sacs, matching the shape of the caudodorsal parts of the premaxillar bones, are appearing with a low dark signal on a MPR DP VISTA image (Fig. 7). This same MRI acquisition allows to visualize the nasofrontal sacs (Fig. 4b).

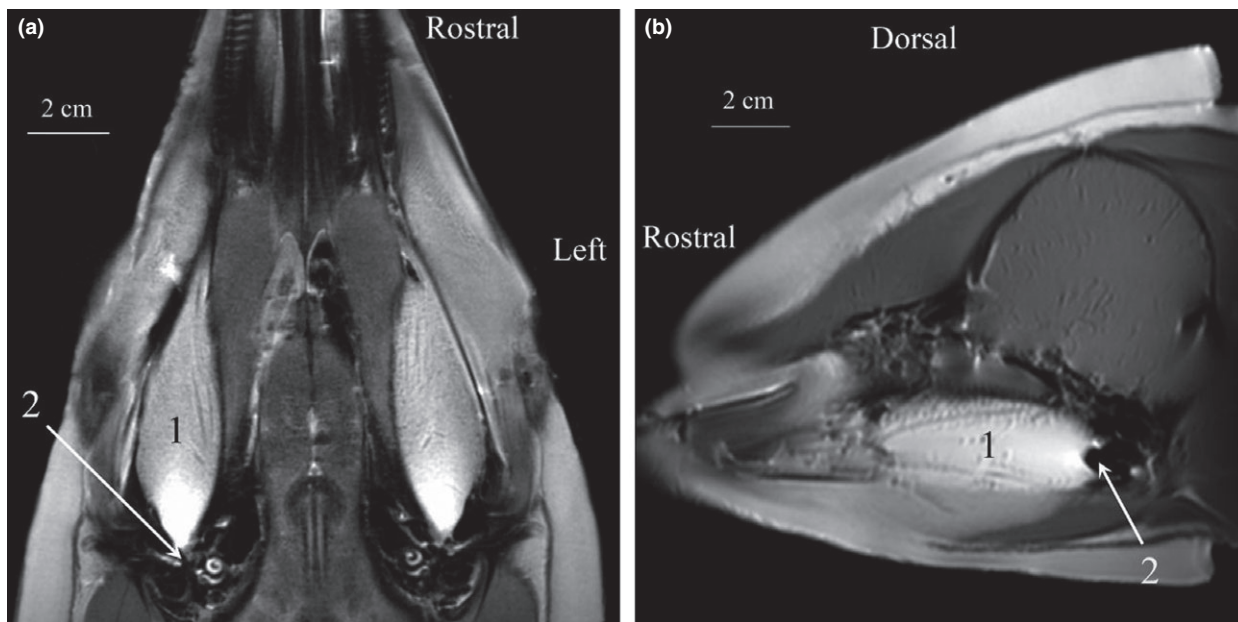


Fig. 3. *Mandibula bulba*. Fatty tissues are directly surrounding the middle ear. (a) DP VISTA acquisition. Frontal section of a fresh common dolphin head (ventral view). (b) T1 SE acquisition. Parasagittal section of a fresh common dolphin head (left view). 1: *Mandibula bulba*, 2: pars tympanica (os temporale).

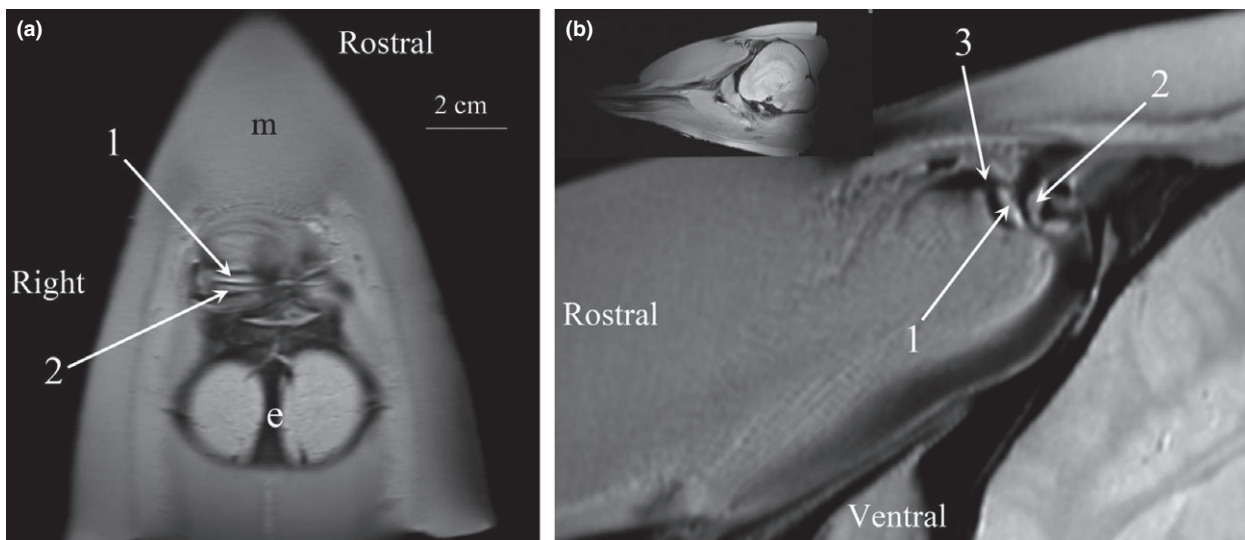


Fig. 4. Monkey lips/dorsal bursae complex (MLDB complex). DP VISTA acquisition. Bursae cantantes highlighted. (a) Frontal section of a fresh common dolphin head (ventral view). (b) Parasagittal section of a fresh common dolphin head (left view). 1: Rostral and right bursae cantantes, 2: caudal and right bursae cantantes, 3: saccus nasofrontalis anterior, m: melon, e: encephalon.

As for adipose tissues and organs, the comparison between fresh and de-frozen heads did not reveal any visible anatomical difference for the nasal respiratory system. The shape, the location and the signals of the nasal diverticula and of the nasal plugs are similarly visualized on MRI images with or without any freezing–thawing cycle (data not shown).

Discussion

Magnetic resonance imaging (MRI) is extensively used in veterinary studies, in particular to describe and study internal anatomy. It allows to analyse organ morphology, organ size and anatomical links with great precision without any of the biases that can arise during dissection. As a non-invasive imaging tool, MRI delivers incomparable visualization of soft tissues (nervous system, muscles, adipose tissues, etc.) and of subtle organ connections. All of the space planes can be illustrated (transverse, frontal and sagittal sections). Moreover, MRI is based on the observation of the nuclear magnetic resonance of protons in water molecules and lipids. Density and biochemical organization of tissues will impact the MRI signal variation. Thus, another advantage of MRI examination is its ability to detect differences in soft tissue on the basis of their biochemical composition. This imaging approach is therefore a tool of choice to study adipose tissues in odontocetes, where minimal biochemical composition differences in the melon have major effects on the function of these tissues (Litchfield et al., 1975).

Medical imaging, in particular computed tomography (CT), has already been used with success to study cetacean anatomy: the nasal respiratory system (Cranford et al., 1996; Houser et al., 2004), the ear (Ketten, 1992), the thoracic region (Alonso-Farré et al., 2014; Ivancic et al., 2014) and the global melon morphology (McKenna et al., 2012) were all analysed using CT scans. MRI was more recently used to describe the neuroanatomy of almost a dozen cetacean species, for example the Atlantic white-sided dolphin (Montie et al., 2007), the harbour porpoise (Marino et al., 2003) and the common dolphin (Marino et al., 2001, 2002). The brain function was recorded by MRI on living dolphins (Ridgway et al., 2006). Other soft tissues of the dolphin's head were also studied using MRI (Rauschmann et al., 2006), and an atlas of the bi-dimensional anatomy of the dolphin's head was constructed by grouping the data coming from the cross sections and corresponding CT and MRI scans (Alonso-Farré et al., 2015). In this atlas, MRI highlighted the soft tissue structures and discriminated the two brain matters, the eye, the larynx, some muscles, fatty tissues and connective tissue, whereas CT scan detected clearly (with hyperdense white signals) the bony structures of the head (skull, ear bones, maxilla, mandibles). However, MRI was used only in a few cases to study adipose tissues in odontocetes despite their major interest in the adaptation to marine life. Only the *bursae cantantes* (described by Cranford, 2000; Cranford et al., 2011) were studied on harbour porpoise MRI images by Huggenberger et al. (2009). These two pairs of fatty tissues, one right and one left for non-Physeteridae odontocetes, were located

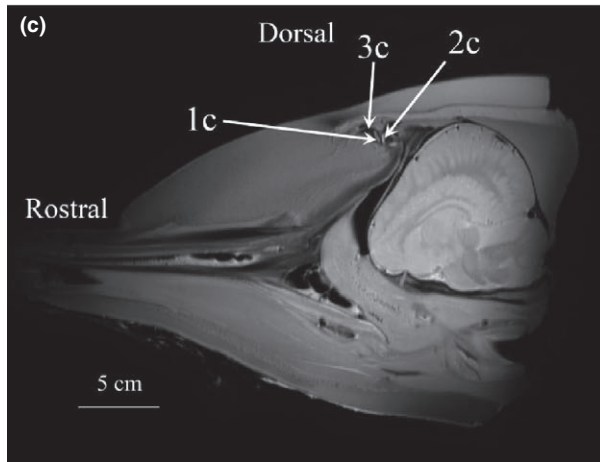
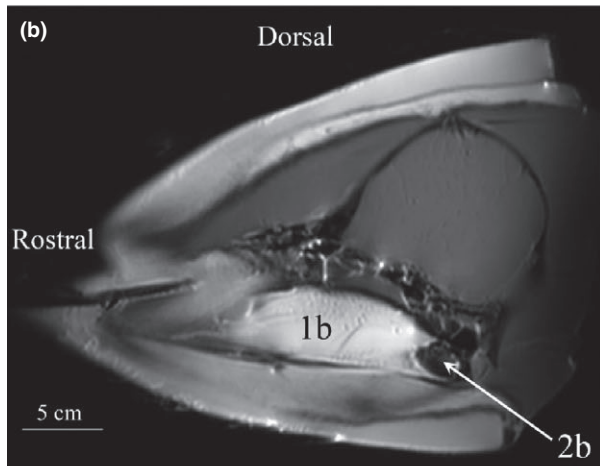
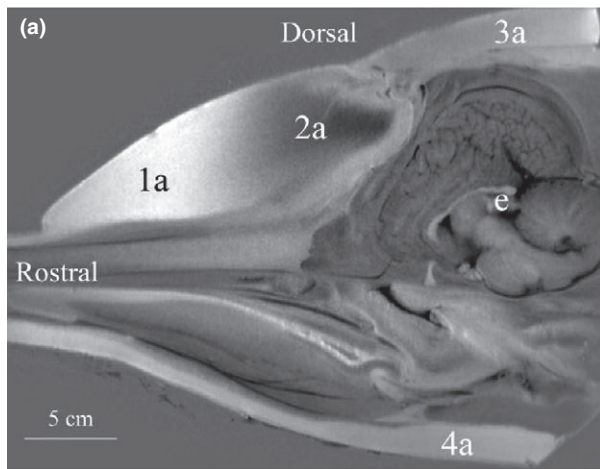


Fig. 5. Fresh and thawed head comparison. (a) T1 IR acquisition. Two distinct parts of the melon/Fig.1a. 1a: outer melon, 2a: inner melon, 3a: dorsal blubber, 4a: ventral blubber, e: encephalon. (b) T1 SE acquisition. *Mandibula bulba* linked to the tympanic part of the temporal bones/Fig. 3b. 1b: *Mandibula bulba*, 2b: pars tympanica (os temporale). (c) DP VISTA acquisition. Bursae cantantes/Fig. 4a. 1c: Rostral and right bursae cantantes, 2c: caudal and right bursae cantantes, 3c: Saccus nasofrontalis anterior, m: melon, e: encephalon.

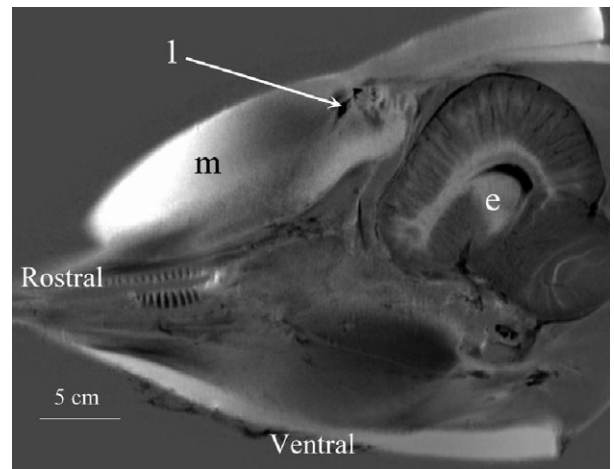


Fig. 6. Vestibular sacs. T1 IR acquisition. Parasagittal section of a fresh common dolphin head (left view). 1: Saccus vestibularis, e: encephalon, m: melon.

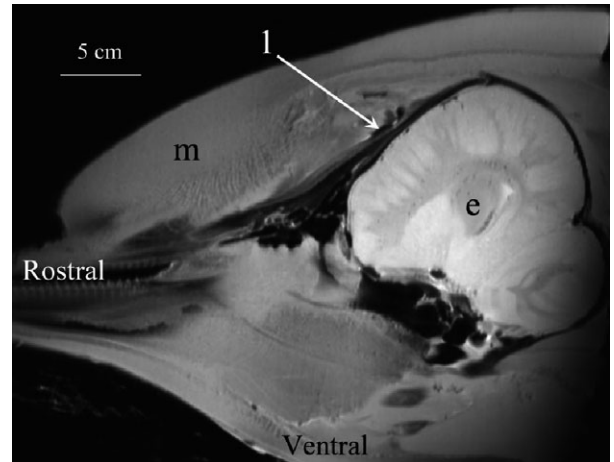


Fig. 7. Premaxillar sacs. DP VISTA acquisition. Parasagittal section of a fresh common dolphin head (left view). 1: Saccus incisivum, e: encephalon, m: melon.

ventrally and caudomedially to the vestibular sacs, dorsally to the premaxillar sacs, rostrally to the anterior nasofrontal sacs and laterally to the nasal passages (paired channels at this height) (Huggenberger et al., 2009). The melon, described from MRI images as a large and symmetrical bulbous fat body rostral to the nasal respiratory system, was not the subject of focused and accurate description in previous studies (Huggenberger et al., 2009; Alonso-Farré et al., 2015). The *mandibula bulba* were illustrated in the study of Alonso-Farré et al. (2015), but its direct connection with the middle ear was not evidenced.

Our study was therefore the first to focus on a MRI analysis of the different types of fatty tissues contained in

the odontocetes head, with the example of a common dolphin. First, we highlighted all the fatty tissues of the dolphin's head on MRI images, using different acquisition parameters: the melon, the *bursae cantantes*, the *mandibula bulba* and the blubber were all clearly identified, as well as their connection with surrounding tissues. We illustrated and confirmed on MRI images (1) the direct connection of the melon with the *bursae cantantes*, (2) the location of the different nasal sacs for either side of the *bursae cantantes*, along the nasal passages and (3) the direct association of the *mandibula bulba* to the middle ear, part of the tympano-periotic complex not welded to the temporal bone (Ognard et al., 2014). To our knowledge, this direct connection is deciphered here with an unprecedented level of precision.

In addition, we were able to discriminate different parts of the melon on the basis of the MRI signals: the part on the melon corresponding to the inner melon (as proposed by Litchfield et al., 1973) appeared as darker when compared to the outer melon and the blubber (especially with T1 IR acquisition, DP VISTA or T2 acquisition, T1 SE acquisition). This differential signal is most likely due to the difference in fatty acid contents, the inner melon containing specifically the so-called acoustic fats, rich in short-branched fatty acids (Litchfield et al., 1973; Koopmann et al., 2003; Zahorodny Duggan et al., 2009). Our results are in perfect correlation with those of McKenna et al. (2012) and Houser et al. (2004), who used CT scans to detect variations of densities within the melons of different odontocetes. We also confirmed the topological anatomical organization of the melon in two parts, the inner one, of lower density, being in all probability responsible of the sound transmission from the MLBD complex to the surrounding environment. Our MRI approach thus still confirmed, if required, the existence of this inner central melon. MRI offers clearly new possibilities for the study of the melon topology, organization and functioning, in particular in terms of comparison between different species of odontocetes, as it allows to discriminate the different internal parts of the organ on the basis of their composition. This composition is closely linked to the sound conduction, and delineating the shape of the inner melon is therefore directly relevant to understand the functioning of echolocation.

Imaging studies are performed on opportunistic samples, such as dead stranded or by-caught cetaceans. Often, the carcasses are frozen until analysis (e.g. Huggenberger et al., 2009; Yamato et al., 2012). CT scans, analysing mainly hard tissues and performed on frozen bodies, are clearly not influenced by freezing. But MRI has to be performed on thawed bodies, especially for fatty tissue analyses. Indeed, the signal of the fatty tissues disappears, on the pondered sequences T2, if the body temperature is

inferior to 20°C (Kobayashi et al., 2010). Furthermore, MRI performed on thawed bodies brought to room temperature and mainly studying soft tissues may be more influenced by previous freezing/thawing cycles. The thaw impact can vary according to the nature of the tissue, the species and the purpose of the examination. MRI images can be modified by the freeze–thaw (e.g. Pownder et al., 2015) or not (e.g. Chang et al., 2014). Our comparative study between the results obtained with a common dolphin stranded dead a few days before analysis and kept unfrozen at 4°C, and the same dolphin, frozen immediately after the first analysis and studied again, using the same protocol, some weeks after, proved that frozen samples can be used with a good confidence to study fatty tissue organization and anatomy in odontocete heads. The fatty tissues (melon, MLBD, mandibular fat and blubber) and the nasal respiratory system showed no differences before and after freezing, in terms of shape of the organs, type and intensity of signal emitted, and in terms of visualization of links with surrounding tissues.

We have proved that the fatty tissues of the odontocete head can be studied with a high level of resolution using MRI approaches. Further deciphering of fatty tissue organization in the odontocete head will therefore be easier to perform, allowing interspecies comparisons, and comparison at different life stages. Knowledge already obtained by others using different approaches (Cranford et al., 1996; Huggenberger et al., 2009; McKenna et al., 2012) will be extended by such MRI-based analyses, thus increasing our level of understanding of how echolocation works in odontocetes.

Acknowledgements

The sample used in this study was collected in the framework of the French Stranding Network (coordinated by Pelagis, La Rochelle, France) and stored at Océanopolis (Brest, France). We thank Aurore Lambert, Claire Bonneville and Eric Alfonsi for their participation in this study. The authors are very grateful to the MR technologists team. A special acknowledgement goes to Philippe Sebert (UBO) and Luc Bressollette (CHRU-UBO). Finally, we thank Ian Nicholson for proofreading this study.

References

- Alonso-Farré, J. M., M. Gonzalo-Orden, J. D. Barreiro-Vázquez, J. M. Ajenjo, A. Barreiro-Lois, M. Llarena-Reino, and E. Degollada, 2014: Cross-sectional anatomy, computed tomography and magnetic resonance imaging of the thoracic region of common dolphin (*Delphinus delphis*) and striped dolphin (*Stenella coeruleoalba*). *Anat. Histol. Embryol.* **43**, 221–229.

- Alonso-Farré, J. M., M. Gonzalo-Orden, J. D. Barreiro-Vázquez, A. Barreiro-Lois, M. André, M. Morell, M. Llarena-Reino, T. Monreal-Pawlowsky, and E. Degollada, 2015: Cross-sectional anatomy, computed tomography and magnetic resonance imaging of the head of common dolphin (*Delphinus delphis*) and striped dolphin (*Stenella coeruleoalba*). *Anat. Histol. Embryol.* **44**, 13–21.
- Bagge, L. E., H. N. Koopman, S. A. Rommel, A. McLellan, and D. A. Pabst, 2012: Lipid class and depth-specific thermal properties in the blubber of the short-finned pilot whale and the pygmy sperm whale. *J. Exp. Biol.* **215**, 4330–4339.
- Blomberg, J., 1978: Functional aspects of odontocete head oil lipids with special reference to pilot whale head oil. *Prog. Chem. Fats Other Lipids.* **16**, 257–278.
- Chang, E. Y., W. C. Bae, S. Statum, J. Du, and C. B. Chung, 2014: Effects of repetitive freeze-thawing cycles on T2 and T2* of the achilles tendon. *Eur. J. Radiol.* **83**, 349–353.
- Cranford, T. W., 2000: In search of impulse sound sources in Odontocetes. In: *Hearing by Whales and Dolphins* (Springer Handbook of Auditory Research Series). (W. W. L. Au, A. N. Popper and R. R. Fay, eds). New York: Springer-Verlag. pp. 109–156.
- Cranford, T. W., M. Amundin, and K. S. Norris, 1996: Functional morphology and homology in the odontocete nasal complex: implications for sound generation. *J. Morphol.* **228**, 223–285.
- Cranford, T. W., W. R. Elsberry, W. G. Van Bonn, J. A. Jeffress, M. S. Chaplin, D. J. Blackwood, D. A. Carder, T. Kamolnick, M. A. Todd, and S. H. Ridway, 2011: Observation and analysis of sonar signal generation in the bottlenose dolphin (*Tursiops truncatus*): evidence for two sonar sources. *J. Exp. Biol.* **407**, 81–96.
- Gardner, S. C., and U. Varanasi, 2003: Isovaleric acid accumulation in odontocete melon during development. *Naturwissenschaften.* **90**, 528–531.
- Genu, A., G. Koch, D. Colin, S. Aho, E. Pearson, and D. Ben Salem, 2014: Factors influencing the occurrence of a T2-STIR hypersignal in the lumbosacral adipose tissue. *Diagn. Interv. Imaging.* **95**, 283–288.
- Houser, D. S., J. Finneran, D. Carder, W. Van Bonn, C. Smith, C. Hoh, R. Mattrey, and S. Ridgway, 2004: Structural and functional imaging of bottlenose dolphin (*Tursiops truncatus*) cranial anatomy. *J. Exp. Biol.* **207**, 3657–3665.
- Huggenberger, S., M. A. Rauschmann, T. J. Vogl, and H. H. A. Oelschläger, 2009: Functional morphology of the nasal complex in the harbor porpoise (*Phocoena phocoena* L.). *Anat. Rec.* **292**, 902–920.
- International Committee on Veterinary Gross Anatomical Nomenclature. (2012) *Nomina anatomica veterinaria* fifth edition (revised version). The Editorail Comittee Hannover (Germany), Columbia, MO (U.S.A.), Ghent (Belgium), Sapporo (Japan).
- Ivancic, M., M. Solano, and C. R. Smith, 2014: Computed tomography and cross-sectional anatomy of the thorax of the live bottlenose dolphin (*Tursiops truncatus*). *Anat. Rec.* **297**, 901–915.
- Jung, J.-L., E. Stephan, M. Louis, E. Alfonsi, C. Liret, F. G. Carpentier, and S. Hassani, 2009: Harbour porpoises (*Phocoena phocoena*) in north-western France: aerial survey, opportunistic sightings and strandings monitoring. *JMBA.* **89**, 1045–1050.
- Ketten, D. R., 1992: The Cetacean Ear: Form, Frequency, and Evolution, in Thomas J. Thomas, R. Kastelein and A. Supin (eds.), *Marine Mammal Sensory Systems*. New York and London: Plenum Press. pp. 53–75.
- Kloepper, L. N., P. E. Nachtigall, M. J. Donahue, and M. Breese, 2012: Active echolocation beam focusing in the false killer whale, *Pseudorca crassidens*. *J. Exp. Biol.* **215**, 1306–1312.
- Kobayashi, T., S. Shiotani, K. Kaga, H. Saito, K. Saotome, K. Miyamoto, M. Kohno, K. Kikichi, H. Hayakawa, and K. Homma, 2010: Characteristic signal intensity changes on post-mortem magnetic resonance imaging of the brain. *Jpn. J. Radiol.* **28**, 8–14.
- Koopman, H. N., S. J. Iverson, and A. J. Read, 2003: High concentrations of isovaleric acid in the fats of odontocetes: variation and patterns of accumulation in blubber vs. stability in the melon. *J. Comp. Physiol. B.* **173**, 247–261.
- Koopman, H. N., 2007: Phylogenetic, ecological, and ontogenetic factors influencing the biochemical structure of the blubber of odontocetes. *Mar. Biol.* **151**, 277–291.
- Koopman, H. N., and Z. P. Zahorodny, 2008: Life history constrains biochemical development in the highly specialized odontocetes echolocation system. *Biol. Sci.* **275**, 2327–2334.
- Koopman, H. N., D. A. Pabst, W. A. McLellan, R. M. Dillaman, and A. J. Read, 2002: Changes in blubber distribution and morphology associated with starvation in the harbour porpoise (*Phocoena phocoena*): evidence for regional differences in blubber structure and function. *Physiol. Biochem. Zool.* **75**, 498–512.
- Landis, J. R., and G. K. Gary, 1977: The measurement of observer agreement for categorical data. *IBS.* **33**, 159–174.
- Litchfield, C., R. Karol, and A. J. Greenberg, 1973: Compositional topography of melon lipids in the Atlantic bottlenosed dolphin *Tursiops truncatus*: Implications for echolocation. *Mar. Biol.* **23**, 165–169.
- Litchfield, C., A. J. Greenberg, and D. K. Caldwell, 1975: Comparative lipid patterns in acoustical and nonacoustical fatty tissues of dolphins, porpoises and toothed whales. *Comp. Biochem. Physiol. B.* **50B**, 591–597.
- Marino, L., T. L. Murphy, L. Gozal, and J. I. Johnson, 2001: Magnetic resonance imaging and three-dimensional reconstructions of the brain of a fetal common dolphin, *Delphinus delphis*. *Anat. Embryol.* **203**, 393–402.
- Marino, L., K. D. Sudheimer, D. Pabst, W. A. McLellan, D. Filsoof, and J. I. Johnson, 2002: Neuroanatomy of the common dolphin (*Delphinus delphis*) as revealed by Magnetic Resonance Imaging (MRI). *Anat. Rec.* **268**, 11–429.
- Marino, L., K. Sudheimer, D. Sarko, G. Sirpenski, and J. I. Johnson, 2003: Neuroanatomy of the harbor porpoise

- (*Phocoena phocoena*) from magnetic resonance images. *J. Morphol.* **257**, 308–347.
- McKenna, M. F., T. W. Cranford, A. Berta, and N. D. Pyenson, 2012: Morphology of the odontocete melon and its implications for acoustic function. *Mar. Mam. Sci.* **28**, 690–713.
- Montie, E. W., G. E. Schneider, D. R. Ketten, L. Marino, K. E. Touhey, and M. E. Hahn, 2007: Neuroanatomy of the subadult and fetal brain of the Atlantic white-sided dolphin (*Lagenorhynchus acutus*) from in situ Magnetic Resonance Images. *Anat. Rec.* **290**, 1459–1479.
- Ognard, J., E. Alfonsi, J.-L. Jung, S. Hassani, P. Meriot, and D. Ben Salem, 2014: Anatomie comparée de l'oreille en scanner et des voies de l'audition en IRM chez le marsouin commun. *J. Neuroradiol.* **41**, 40–41.
- Pownder, S. L., P. H. Shah, H. G. Potter, and M. F. Koff, 2015: The effect of freeze-thawing on magnetic resonance imaging T2* of freshly harvested bovine patellar tendon. *Quant. Imaging Med. Surg.* **5**, 368–373.
- Rauschmann, M. A., S. Huggenberger, L. S. Kossatz, and H. A. A. Oelschläger, 2006: Head morphology in perinatal dolphins: a window into phylogeny and ontogeny. *J. Morphol.* **267**, 1295–1315.
- Read, A. J., P. R. Wiepkema, and P. E. Nachtigall, 1997: *The Biology of the Harbour Porpoise*. Woerden, The Netherlands: De Spil Publishers. pp. 90–166.
- Régis-Arnaud, A., B. Guiu, P. M. Walker, D. Krausé, F. Ricolfi, and D. Ben Salem, 2011: Bone marrow fat quantification of osteoporotic vertebral compression fractures: comparison of multi-voxel proton MR spectroscopy and chemical-shift gradient-echo MR imaging. *Acta Radiol.* **52**, 1032–1036.
- Ridgway, S., D. Houser, J. Finneran, D. Carder, M. Keogh, W. Van Bonn, C. Smith, M. Scadeng, D. Dubowitz, R. Mattrey, and C. Hoh, 2006: Functional imaging of dolphin brain metabolism and blood flow. *J. Exp. Biol.* **209**, 2902–2910.
- Yamato, M., D. R. Ketten, J. Arruda, S. Cramer, and K. Moore, 2012: The auditory anatomy of the minke whale (*Balaenoptera acutorostrata*): a potential fatty sound reception pathway in a baleen whale. *Anat. Rec.* **295**, 991–998.
- Zahorodny Duggan, Z. P., H. N. Koopman, and S. M. Budge, 2009: Distribution and development of the highly specialized lipids in the sound reception systems of dolphins. *J. Comp. Physiol. B.* **179**, 783–798.